# Experimental evidence of localized plasmon resonance in composite materials containing single-wall carbon nanotubes

M. V. Shuba, A. G. Paddubskaya, A. O. Plyushch, P. P. Kuzhir, G. Ya. Slepyan, and S. A. Maksimenko
*Institute for Nuclear Problems, Belarus State University, Bobruiskaya 11, 220050 Minsk, Belarus*

V. K. Ksenevich and P. Buka
*Department of Physics, Belarus State University, Nezalezhnastsi Avenue 4, 220030 Minsk, Belarus*

D. Seliuta, I. Kasalynas, J. Macutkevic, and G. Valusis
*Center for Physical Sciences and Technology, A. Gostauto 11, LT-01108 Vilnius, Lithuania*

C. Thomsen
*Institut für Festkörperphusik, Technische Universität Berlin, Hardenbergstraße 36, D-10623 Berlin, Germany*

A. Lakhtakia
*Nanoengineered Metamaterials Group, Department of Engineering Science and Mechanics, Pennsylvania State University, University Park, Pennsylvania 16802-6812, USA*

(Received 25 December 2011; revised manuscript received 19 March 2012; published 18 April 2012)

Experimental proof of localized plasmon resonance was found in thin films containing either single-walled carbon nanotubes (SWNT) or SWNT bundles of different length. All samples were prepared by a simple technique that permitted the selection of different SWNT lengths in different samples without significant differences in electronic properties. Fourier-transform infrared spectroscopy showed that an optical-density peak, the same as a terahertz conductivity peak, shifts to higher frequencies as the SWNT lengths are reduced—in agreement with a similar tendency predicted for the localized plasmon resonance in finite-length SWNTs [Slepyan *et al.*, Phys. Rev. B **81**, 205423 (2010)].

DOI: 10.1103/PhysRevB.85.165435 PACS number(s): 73.20.Mf, 42.70.−a, 73.25.+i, 78.67.Ch

## I. INTRODUCTION

A single-wall carbon nanotube (SWNT) is a sheet of hexagonally arranged carbon atoms rolled up into a cylinder. It can be either metallic or semiconducting, depending on its chirality.[1] The axial surface conductivity of a metallic SWNT in the far-infrared (FIR) and subterahertz spectral regimes is described well by the Drude equation.[2] The curvature of a metallic SWNT in the transverse plane leads to the appearance of a small band gap,[3] leading to a departure of the axial surface conductivity from the Drude equation at low frequencies. However, if the band-gap energy is smaller than or comparable to the energy of thermal motion ($= k_B T$, where $k_B$ is the Boltzmann constant and $T$ is the absolute temperature), then the low-frequency conductivity is determined mostly by intraband electron transition, and the departure from the Drude equation is negligibly small.[4] In other words, at a typical[3] band-gap value $\simeq 10$ meV, a SWNT acts like a metallic tube at room temperature.

The electromagnetic responses of an individual SWNT and of composite materials containing SWNT inclusions depend critically in the terahertz and subterahertz regimes on the SWNT length.[4–10] Arising from the strong retardation[2] of surface waves, length-dependent antenna resonances of a metallic SWNT in the FIR regime have been predicted.[5–7] In optics parlance, each of these surface waves is a surface plasmon-polariton (SPP) wave and each antenna resonance is a localized plasmon resonance.

A broad peak has been observed in the conductivity spectrum of composite materials containing nominally identical SWNTs.[11–17] Typically, the frequency $f_p$ of this peak is located in the range $f_p/c \in [50,200]$ cm$^{-1}$, where $c$ is the speed of light.

Some research groups[4,11] have suggested that the localized plasmon resonance is responsible for this terahertz conductivity peak (TCP), with $f_p$ depending on the length of the SWNTs. In contrast, other researchers[12,14–17] have suggested that the TCP is a result of an interband transition in small-gap SWNTs. Then $f_p$ must depend on the diameter of the SWNTs, the experimental observation of this dependence being explicitly claimed in Refs. 14 and 17. However, the length of SWNTs in those experiments was not controlled.

Thus, at present, a single opinion about the mechanism behind the TCP exhibited by the SWNT-containing composite materials does not exist.[4,17,18] As theoretically shown in Ref. 4, both effects—the interband transition and the localized plasmon resonance—contribute simultaneously and cause the appearance of *only one* conductivity peak; moreover, at room temperature the contribution of localized plasmon resonance prevails.

So, in order to clarify the physical mechanism of the TCP, definitive experiments on the dependence of this peak on the SWNT length are needed. In this paper, we experimentally show the length dependence of $f_p$ for SWNT films comprising either isolated SWNTs or SWNT bundles. For short SWNTs (about 200 nm in length), we found that $f_p/c \simeq 1000$ cm$^{-1}$ (in contrast to previous experiments[11,12,14–17] for which $f_p/c \leqslant 200$ cm$^{-1}$). Our experimental data are in good agreement with our theoretical calculations based on the model of localized plasmon resonance in SWNTs.[4]

 

## II. MATERIALS AND METHODS

Three types of purified SWNT materials were used in our experiments: (1) electric-arc-produced SWNT bundles (A-SWNT, CarboLex, Inc.) obtained using nickel-yttrium catalyst, with SWNT diameters ranging from 1.2 to 1.5 nm and purity between 50% and 70%; (2) isolated SWNTs (C-SWNT, SWeNT, Inc.) produced by chemical vapor deposition (CVD) on a cobalt-molybdenum catalyst, with average SWNT diameter 1 nm and purity exceeding 75%; and (3) SWNT bundles (H-SWNT, Nano-C, Inc.) produced by gas-phase catalysis (HiPco process), with average SWNT diameter 1.1 nm and purity exceeding 95%.

In order to obtain SWNTs of a fixed length, we developed a SWNT-cutting technique based on acid treatment[19] with subsequent SWNT extraction from the acid.[20] Contrary to the frequently used acid-cutting method,[21] we used a low-temperature (8 °C) ultrasonic acid treatment for time $t$. The low temperature prevents the SWNT wall from degradation by the acid, whereas the same treatment at a temperature exceeding 30 °C degrades the SWNT wall, thereby leading to very strong departures from the Drude equation. For one sample (labeled H4 in Table I), we cut SWNTs by ultrasonication of 0.5 mg SWNT material in 5 ml of N,N-dimethylformamide (DMF) at 8 °C for 40 h.

Homogeneous SWNT suspensions were obtained by ultrasonication (44 kHz at ultrasonic intensity 70 W $cm^{-2}$) for 4 h—in isopropanol (IP) for C- and H-SWNTs, or in DMF for A-SWNTs. Thin SWNT films of thickness $d \in [100,500]$ nm were prepared by spraying the suspensions on heated (120 °C for SWNT-IP suspensions and 180 °C for SWNT-DMF suspensions) silicon substrates. In order to avoid agglomeration of SWNTs (formation of the thick bundles from individual tubes and thinner bundles) during film preparation we (i) prepared SWNT suspensions of low concentration ($< 10^{-3}$ g $l^{-1}$), (ii) employed continuous powerful ultrasonic stirring of the suspensions during spraying, and (iii) heated silicon substrates to quickly evaporate the solvent.

An atomic force microscope (AFM, Solver P47 PRO, NT-MDT, Inc.) was used to study size distributions of the SWNTs in each sample. Several drops of the SWNT-DMF (SWNT-IP) suspension were deposited on a freshly prepared mica surface at 190 °C (120 °C). After the solvent had evaporated, each sample for AFM examination was heated in vacuum ($10^{-6}$ Torr) at 500 °C for 1 h in order to evaporate any residual solvent and other organic impurities.

AFM images of C-SWNT films showed that we were able to prevent the formation of thick bundles; thus, most of the C-SWNTs were isolated from each other, though bundles with diameter less than 4 nm were formed. Comparison of the AFM images of different samples also demonstrated that the average bundle diameter of C-SWNTs is smaller than the average bundle diameters of A-SWNTs and H-SWNTs. The details of prepared samples and their designation are provided in Table I.

With normally incident light, the spectra of optical density (or absorbance) were obtained for $f/c \in [25,7400]$ $cm^{-1}$ with a resolution of 10 $cm^{-1}$, using a commercial Fourier-transform infrared (FT-IR) spectrometer (Nicolet-8700, Nicolet Instrument Corporation, $f/c \in [200,7400]$ $cm^{-1}$) and a customized vacuum FT-IR spectrometer ($f/c \in [20,400]$ $cm^{-1}$). Raman measurements were performed with the Raman microscope LabRam HR800 (Horiba Jobin Yvon, Inc.) and 632.8-nm laser line excitation.

TABLE I. Details of the samples prepared. $L_m$ and $\Delta$ are the mean and the standard deviation, respectively, of the SWNT length for distributions presented in Figs. 1(a)–1(d), 2(a)–2(c), and 3(a)–3(c).

| Sample label | SWNT type | $t$ (h) | $L_m$ ($\mu$m) | $\Delta$ ($\mu$m) | $f_p/c$ ($cm^{-1}$) |
|---|---|---|---|---|---|
| H1 | H-SWNT | 0 | 0.75 | 0.41 | 260 |
| H2 | H-SWNT | 10 | 0.24 | 0.10 | 600 |
| H3 | H-SWNT | 30 | 0.18 | 0.08 | 1020 |
| H4[a] | H-SWNT | 40 | 0.37 | 0.23 | 380 |
| A1 | A-SWNT | 0 | 1.08 | 0.56 | 150 |
| A2 | A-SWNT | 10 | 0.41 | 0.15 | 380 |
| A3 | A-SWNT | 30 | 0.15 | 0.07 | 1070 |
| C1 | C-SWNT | 0 | 0.61 | 0.46 | 170 |
| C2 | C-SWNT | 20 | 0.33 | 0.16 | 420 |
| C3 | C-SWNT | 30 | 0.17 | 0.12 | 530 |

[a]Sample H4 was ultrasonicated in DMF for 40 h.

## III. EXPERIMENTAL RESULTS

Figures 1(a)–1(d) shows the length distributions of the H-SWNT bundles in Samples H1–H4 obtained from AFM images. From this figure and the data in Table I, we conclude that all four samples have different length distributions. AFM images also show that the diameters of acid-cut bundles vary from 3 to 10 nm, implying that the number of SWNTs in a bundle varies from 2 to 40. Before acid treatment, bundle diameters were found to be $\leqslant 20$ nm.

Figure 1(e) shows the optical-density spectra for samples H1–H4. Each sample displays in the Drude regime ($f/c < 3000$ $cm^{-1}$) a broad absorbance peak whose central frequency $f_p$ is presented in Table I. Significantly, $f_p$ is larger when the SWNTs are shorter. However, $f_p$ is not directly proportional to the mean length $L_m$, because the electromagnetic responses of longer SWNTs are more intense than those of shorter SWNTs. Hence, the longer SWNTs in a given sample (with length $L > L_m$) contribute far more to the formation of the TCP than the shorter SWNTs in that sample. The observed length dependence of $f_p$ is in accord with the proposal in Refs. 7 and 11—and therefore validates that the mechanism underlying the TCP is localized plasmon resonance. This length dependence of $f_p$ remains whether acid was used to cut the SWNTs (H1–H3) or not (H4), with the value of $f_p$ for H4 intermediate to those for H1 (longer SWNTs) and H2 (shorter SWNTs).

In order to confirm that $f_p$ is determined primarily by the SWNT length rather than the SWNT diameter, we shifted attention to samples A1–A3 (comprising SWNT bundles with SWNT average diameter 1.4 nm) and C1–C3 (comprising isolated SWNTs of average diameter 1 nm). Length distributions are presented in Figs. 2(a)–2(c) and 3(a)–3(c), while optical-density spectra are shown in Figs. 2(d) and 3(d). For each of two families of the samples, we see that $f_p$ increases as the SWNT lengths decrease. This dependence holds even when all seven samples (H1–H4 and A1–A3) containing bundled SWNTs are considered together.

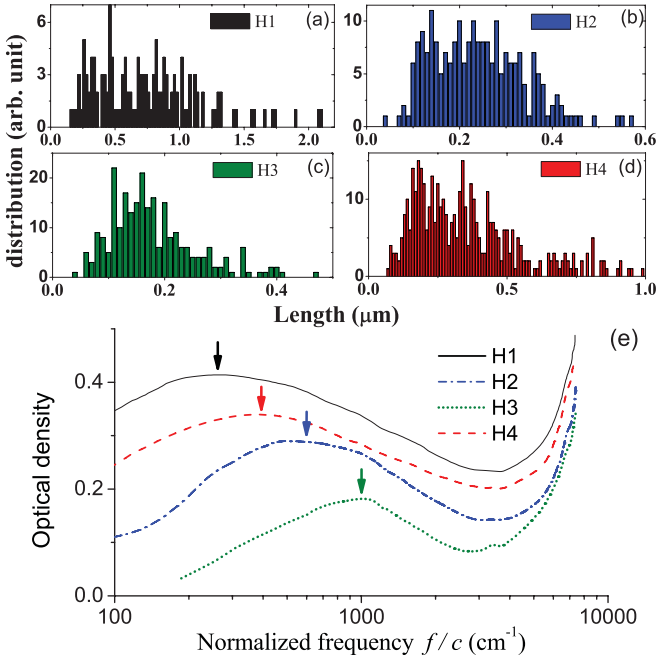


FIG. 1. (Color online) Length distributions of SWNT bundles in samples (a) H1, (b) H2, (c) H3, and (d) H4. (e) Optical-density spectra of these samples. All spectra except for H3 have been normalized (in order to be approximately similar) for $f/c \in [3000, 7400]$ cm$^{-1}$ and offset for clarity. Un-normalized spectra are available in the Supplemental Material.[22] Arrows indicate the TCPs.

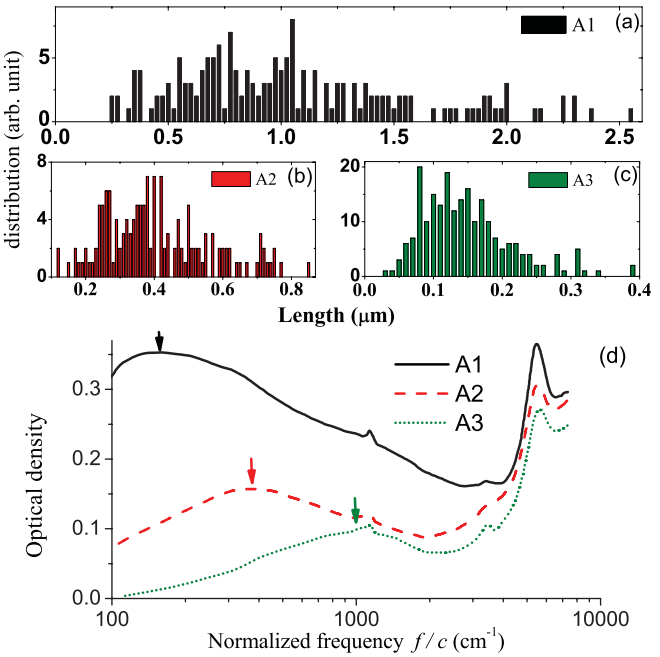


FIG. 2. (Color online) Same as Fig. 1, but for samples A1, A2, and A3. Unnormalized spectra are available in the Supplemental Material.[22]

Comparison of data for sample C3 with data for samples H3 and A3 in Table I shows immediately that $f_p$ is lower for films containing isolated SWNTs than for films containing SWNT bundles, if the length distributions are roughly the same. This trend agrees with a prediction[10] based on the theory of localized plasmon excitation: the SPP wave has stronger retardation in an isolated SWNT than in an SWNT bundle, so that localized plasmon resonance in an isolated SWNT occurs at a lower frequency than in a SWNT bundle.

The first interband transition in semiconducting SWNTs does not disappear after treatment by the acid. This may be seen by the optical-density peaks at $f/c \simeq 5500$ cm$^{-1}$ for all three samples in Fig. 2(d). Thus the innate transport characteristics of SWNTs are disturbed only weakly by the acid treatment.

The TCP shift is accompanied with a decrease in its intensity for all types of SWNTs. Significant intensity reduction in the optical-density spectra in the FIR regime can be explained by two effects. The first is that shorter SWNTs are weaker scatterers, as demonstrated by Fig. 6 in Sec. IV. The second is the damage of SWNT sidewalls, which will decrease the electron relaxation time and therefore the FIR conductivity of the SWNT films.[23,24]

Raman spectroscopy is frequently used for qualitative estimation of defects or other symmetry-breaking elements in SWNTs. Figure 4 shows the Raman spectra of SWNTs of different types before and after acid cutting for 30 h. The dominant feature is a high-frequency $G$ band (1550–1600 cm$^{-1}$) with a double-peak structure, which originates from tangential vibrational modes of $sp^2$-hybridized carbon atoms.[25] Also in each spectrum is the $D$ band (1306–1323 cm$^{-1}$), which is associated with disorder-induced symmetry-lowering effects. A comparative analysis of defect density can be made using the ratio $I_D/I_G$, where $I_D$ is the area of the $D$ band in the Raman spectrum and $I_G$ that of the $G$ band.[25]

According to Figs. 4(b) and 4(c), the ratio $I_D/I_G$ increases from 0.1 (for A1 and C1) up to 0.35 (for A3 and C3); i.e., acid

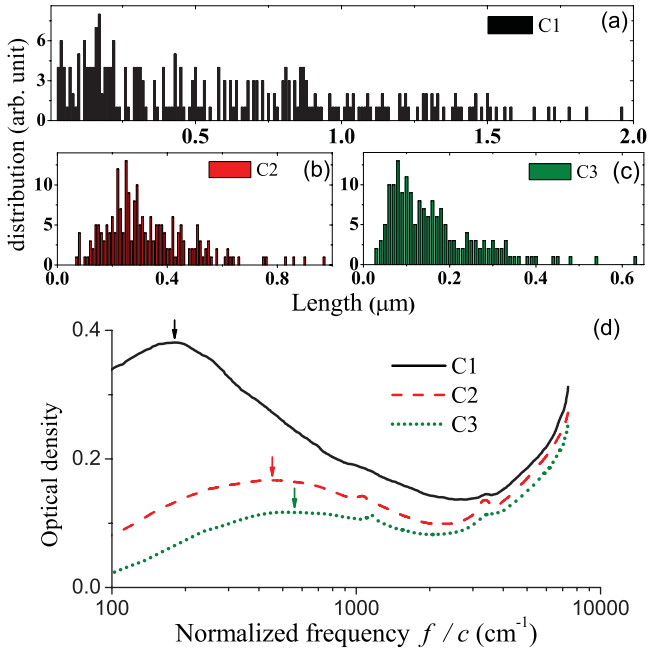


FIG. 3. (Color online) Same as Fig. 1, but for samples C1, C2, and C3. These samples comprise isolated SWNTs instead of SWNT bundles. Unnormalized spectra are available in the Supplemental Material.[22]

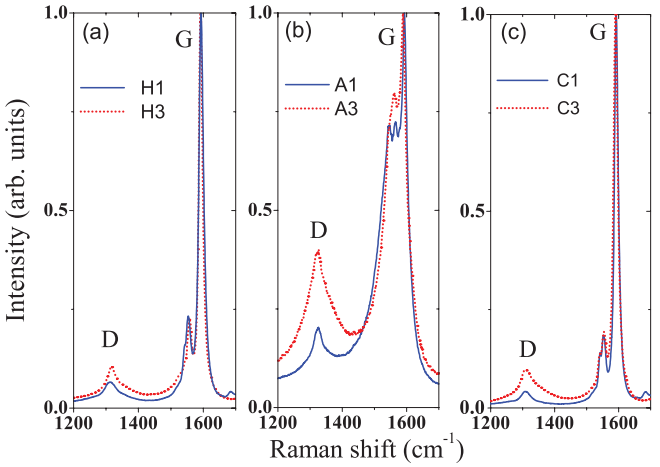


FIG. 4. (Color online) $D$ and $G$ bands in the Raman spectra (633 nm excitation) of samples (a) H1 and H3, (b) A1 and A3, (c) C1 and C3. Spectra are normalized to the value at the peak frequency of the $G$ band.

cutting for 30 h increases that ratio. For samples H1 ($t = 0$) and H3 ($t = 30$ h) in Fig. 4(a), however, the ratio does not have significantly different values. We stress that absolute value of $I_D/I_G$ (about 0.3) obtained for SWNT films containing short SWNTs is not high, and is in fact comparable with the value of $I_D/I_G$ for separated short SWNTs obtained by size-exclusion chromatography.[26]

We carried out additional experiments to relate the TCP intensity to the value of $I_D/I_G$. Short SWNTs (the same as were used for H3 sample preparation) were ultrasonicated in the same acid mixture at 25 °C for 3 h in order to increase the number of defect sites in SWNTs. The value of $I_D/I_G$ thereby increased up to 1.4, but $f_p/c$ remained at 1000 cm$^{-1}$ although the TCP peak did lower.

Raman spectroscopy has thus demonstrated that acid cutting at low temperature in our experiments disturbs their electronic properties quite weakly.

According to Ref. 14, acid treatment leads to p-doping of semiconducting SWNTs, thereby increasing their conductivity. This "metallization" of semiconducting SWNTs in a SWNT bundle increases the phase speed of the eigenwave in the bundle and, consequently, leads to a blue shift of the localized plazmon resonance.[9]

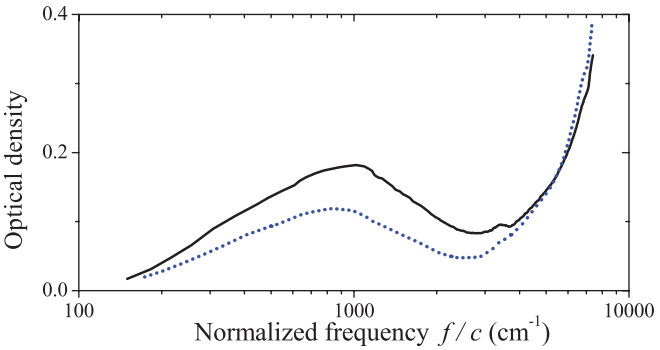


FIG. 5. (Color online) Optical-density spectra of the sample H3 before (solid line) and after (dotted line) heating in vacuum ($10^{-6}$ Torr) for 90 min at 500 °C.

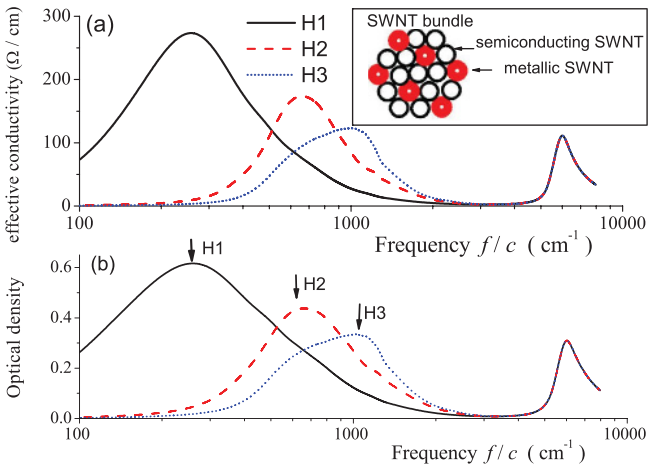


FIG. 6. (Color online) Calculated spectra of (a) effective conductivity $\sigma_{\text{eff}}$ and (b) optical density of samples H1–H3. All bundles are assumed to be identical, as shown in the inset, with bundle diameter 7.2 nm. Each bundle contains 6 metallic zigzag (15,0) and 13 semiconducting (14,0) SWNTs, and the length distributions are the same as for samples H1–H3. Arrows indicate the TCPs.

Doping can lead also to the enhancement of the intertube conductivity.[13] In turn, the depolarizing field in finite-length SWNTs decreases and consequently the low-frequency optical density of SWNT films increases—as was observed in Ref. 13–15 and discussed in Ref. 9. As the optical density increases more at lower frequencies than at higher frequencies, the TCP peak shifts to lower frequencies, as was observed in Refs. 13,17.

Thus both the metallization of semiconducting SWNTs and the enhancement of intertube conductivity can affect the TCP frequency of SWNT thin films.[9] The investigation of the influence of these effects on the frequency of the TCP peak is out of the scope of present work. We only show that the influence of acid in our cutting experiments on the TCP frequency is weaker than the influence of SWNT length.

Figure 5 shows optical density of the samples H3 before and after heating under vacuum ($10^{-6}$ Torr) for 90 min at 500 °C. The pre-heating sample can be considered as doped, and the post-heating sample as undoped. As is evident from Fig. 5, the doped sample has a higher conductivity than the undoped sample, in agreement with the experimental findings of other researchers.[14,15,27,28] Also, from this figure it is clear that the TCP frequency $f_p$ of the sample H3 changes weakly after heating. This proves that $f_p$ depends less on doping than on the SWNT lengths. Additional heating under vacuum for 1 h at temperatures up to 1000 °C did not change the optical density spectrum of the sample H3 as compared with heating at 500 °C. We also observed weak influence of the acid doping during the cutting on the TCP frequency for the samples comprising A-SWNTs and C-SWNTs.

Let us emphasize that TCP shifts with decreasing SWNT lengths have been shown in this section for SWNT films produced and purified by different methods and consequently having different purities. The optical-density FIR spectra of thin films prepared even from raw (as produced, purchased from Nano-C, Inc.) HiPCo SWNTs of different lengths also demonstrate the main features: Drude-like characteristics in

the optical-density spectra and increase of $f_p$ with reduction of SWNT length; see Fig. S5 in the Supplemental Material.[22] Thus we can stress that impurities in our samples (introduced by production and purification methods) cannot negate the observation of the shift of TCP frequency with decreasing SWNT length.

## IV. MODEL CALCULATIONS

Following Ref. 4, we calculated the effective conductivity and refractive index of a thin film comprising randomly dispersed and randomly oriented SWNT bundles. Aiming only at a qualitative comparison of the model results with the experimental data, we set all bundles to have the same cross-sectional radius $R_b = 3.6$ nm. Also, we ignored the metallization of semiconducting SWNTs by acid treatment,[14] as the details of that effect in our experiments are unknown. As shown in Fig. 6, each bundle was taken to comprise 6 metallic zigzag (15,0) and 13 semiconducting (14,0) SWNTs, in accordance with equiprobability of SWNTs of identical radii but different chiral angles. The length distribution was the same as for either H1 or H2 or H3; see Figs. 1(a)–1(c). Let us note that H1 contains thicker bundles ($R_b \approx 20$ nm) than samples H2 and H3 ($R_b \in [3,10]$ nm). Decrease of the bundle diameter leads to a red shift of the localized plasmon resonance, whereas decrease of the bundle length leads to a blue shift.[10] The strong blue shift of TCP in our experiments point outs that the effect of length decrease completely overshadows the effect of bundle-diameter reduction. As the considered model film comprises only bundles of identical diameter, the calculated data can only demonstrate the length dependence of TCP.

The axial surface conductivity $\sigma_{zz}$ of each SWNT was calculated with the application of a tight-binding model for $\pi$-electron motion that takes spatial quantization into account.[2] As was established in Ref. 4 on the basis of experimentally determined temperature dependence of the TCP,[15] the electron relaxation angular frequency $2\pi\nu$ in the Drude regime of SWNT at room temperature is $3 \times 10^{13}$ rad s$^{-1}$. We used $2\pi\nu = 3 \times 10^{13}$ rad s$^{-1}$ and $5 \times 10^{13}$ rad s$^{-1}$ for calculating $\sigma_{zz}$ in the Drude regime and in the range of interband transition, respectively.

Each thin film was taken to be of thickness $d = 200$ nm. The volume fraction occupied by the SWNTs bundles, each conceived as a cylinder of volume $\pi R_b^2 L$, was taken as 0.1. To calculate the polarizability of an SWNT bundle, an integral-equation method which relies on the prescription of effective boundary conditions for the electromagnetic field across the surface of an SWNT[2] was applied; see Appendix A in Ref. 9 for details.

Figure 6 shows the frequency dependence of the effective conductivity $\sigma_{\text{eff}}$ and the optical density of the SWNT films with length distributions the same as for samples H1–H3. The TCP for each of the three model films in Fig. 6(a) coincides with an optical-density peak in Fig. 6(b), both caused by localized plasmon resonance in the SWNTs. Furthermore, the calculated TCP frequency is higher when the SWNT inclusions are shorter, just as determined experimentally for Fig. 1(e).

We also made model computations for thin films containing isolated SWNTs with the same length distributions as for samples C1–C3. In agreement with the experimental data in Fig. 3(d), $f_p/c$ shifted in our model calculations (data not presented here) from 160 cm$^{-1}$ to 500 cm$^{-1}$. So we can conclude that the theory presented in Ref. 4 describes well the observed optical properties of SWNT thin films.

We suppose that in other experiments[11–16] the observed TCP was caused by the depolarizing field in finite-length SWNTs, whereas the influence of interband transition through the small band gap of quasimetallic SWNTs was much smaller. In order to observe the interband transitions in FIR spectra the following two conditions must be fulfilled: $E_b > f_{sp}h$ and $E_b > k_BT$, where $E_b$ is the small band gap caused by curvature in the transverse plane of a SWNT, $h$ is the Planck constant, and $f_{sp}$ is the length-dependent frequency of the localized plazmon resonance in a SWNT. The first condition ($E_b > f_{sp}h$) is invalid for short SWNTs; then, the depolarizing field prevents the excitation of an axial current in the SWNT and the peak at frequency $E_b/h$ does not appear.[4] The second condition ($E_b > k_BT$) was invalid for room-temperature experiments of Refs. 11–15; then, the SWNT conductivity is determined mostly by intraband electron transitions so that the influence of the interband transition on the FIR spectra is weak.[4,29] Thus, in order to observe the small-band-gap transition in SWNTs by means of FIR spectroscopy, low-temperature ($<50$ K) measurements with long SWNTs ($>2$ $\mu$m for isolated SWNTs and $>5$ $\mu$m for SWNT bundles) are necessary; see, for example, Fig. 4 in Ref. 4.

The geometric parameters of the SWNTs in the samples of Ref. 15 are different from those of the SWNTs used in our experiments. This leads to a different spectral location of the TCP in relation to the electron relaxation frequency, and therefore to a different mechanism underlying the TCP formation. In Ref. 15, $f_p = 2.39 \times 10^{12}$ Hz is smaller than the electron relaxation frequency $\nu = 4.78 \times 10^{12}$ Hz, which leads to surface waves with imaginary wavenumbers. Such surface waves do not contribute to density of photonic states—see Appendix B in Ref. 9—and antenna resonances are absent in SWNTs, so that the TCP occurs due to the axial depolarizing field.[4]

In contrast, $f_p$ for all samples considered here exceeds the electron relaxation frequency, so that the surface waves have complex wave numbers whose real parts are dominant. Quasiperiodic oscillations then occur and antenna resonances can be excited. So we stress that the phenomenon of localized plasmon resonance occurs in our samples. The breadth of the TCP is comparable to $f_p$ in magnitude, as a result of inhomogeneous broadening over the SWNT length—i.e., it can be explained by dephasing of individual oscillators in a linear array.

## V. CONCLUSION

Optical density measurements were carried out on thin films containing either SWNTs or SWNT bundles. Low-temperature (8 °C) acid cutting instead of conventional acid cutting at 40 °C accompanied by ultrasonication prevented the chemical degradation of the SWNT wall, and thereby allowed the selection of the range of SWNT lengths in each sample without alteration of electronic properties. The wave number of the optical density peak, which is the same as the terahertz conductivity peak, increased from 150 to 1000 cm$^{-1}$ at room

temperature as the SWNT length was reduced from 1 to 0.15 $\mu$m. The frequency shift of the TCP is attributable to the excitation of localized plasmon resonance and is supported well by calculations for a relevant physical model.

## ACKNOWLEDGMENTS

We are grateful to Rimvydas Venckevicius and Natalya P. Vileishikova for his kind assistance for Fourier spectroscopy, Galina I. Dovbeshko for providing us arc-discharge SWNTs, Lyudmila V. Baran for recording AFM images, and Gediminas Niaura for performing Raman measurements. We thank the Belarusian Inter-University Center of Research Facilities for kind permission to use its AFM. This research was partially supported by the BRFFR under Projects No. F10R-002 and No. F10CO-020; EU FP7 under Projects No. FP7-230778 TERACAN, No. FP7-247007 CACOMEL, and No. FP7-266529 BY-NanoERA; ISTC under Project No. B-1708 and NATO Collaborative Linkage Grant (Reference No. CB-P.EAP.CLG983910); Grant No. MIP-097/2011 from the Research Council of Lithuania; and the Binder Endowment at Penn State.

[1] S. Reich, C. Thomsen, and J. Maultzsch, *Carbon Nanotubes. Basic Concepts and Physical Properties* (Wiley-VCH, Berlin, 2004).
[2] G. Ya. Slepyan, S. A. Maksimenko, A. Lakhtakia, O. Yevtushenko, and A. V. Gusakov, Phys. Rev. B **60**, 17136 (1999).
[3] C. Zhou, J. Kong, and H. Dai, Phys. Rev. Lett. **84**, 5604 (2000).
[4] G. Ya. Slepyan, M. V. Shuba, S. A. Maksimenko, C. Thomsen, and A. Lakhtakia, Phys. Rev. B **81**, 205423 (2010).
[5] G. W. Hanson, IEEE Trans. Antennas Propag. **53**, 3426 (2005).
[6] P. J. Burke, S. Li, and Z. Yu, IEEE Trans. Nanotechnol. **5**, 314 (2006).
[7] G. Ya. Slepyan, M. V. Shuba, S. A. Maksimenko, and A. Lakhtakia, Phys. Rev. B **73**, 195416 (2006).
[8] D. Seliuta, I. Kasalynas, J. Macutkevic, G. Valusis, M. V. Shuba, P. P. Kuzhir, G. Ya. Slepyan, S. A. Maksimenko, V. K. Ksenevich, V. Samuilov, and Q. Lu, Appl. Phys. Lett. **97**, 073116 (2010).
[9] A. M. Nemilentsau, M. V. Shuba, G. Ya. Slepyan, P. P. Kuzhir, S. A. Maksimenko, P. N. D'yachkov, and A. Lakhtakia, Phys. Rev. B **82**, 235424 (2010).
[10] M. V. Shuba, S. A. Maksimenko, and A. Lakhtakia, Phys. Rev. B **76**, 155407 (2007).
[11] N. Akima, Y. Iwasa, S. Brown, A. M. Barbour, J. Cao, J. L. Musfeldt, H. Matsui, N. Toyota, M. Shiraishi, H. Shimoda, and O. Zhou, Adv. Mater. **18**, 1166 (2006).
[12] A. Ugawa, A. G. Rinzler, and D. B. Tanner, Phys. Rev. B **60**, R11305 (1999).
[13] B. Ruzicka, L. Degiorgi, R. Gaal, L. Thien-Nga, R. Bacsa, J.-P. Salvetat, and L. Forro, Phys. Rev. B **61**, R2468 (2000).
[14] M. E. Itkis, S. Niyogi, M. E. Meng, M. A. Hamon, H. Hu, and R. C. Haddon, Nano Lett. **2**, 155 (2002).
[15] F. Borondics, K. Kamarás, M. Nikolou, D. B. Tanner, Z. H. Chen, and A. G. Rinzler, Phys. Rev. B **74**, 045431 (2006).
[16] T. Kampfrath, K. von Volkmann, C. M. Aguirre, P. Desjardins, R. Martel, M. Krenz, C. Frischkorn, M. Wolf, and L. Perfetti, Phys. Rev. Lett. **101**, 267403 (2008).
[17] A. Pekker and K. Kamarás, Phys. Rev. B **84**, 075475 (2011).
[18] M. Muthee, E. Carrion, J. Nicholson, and S. K. Yngvesson, AIP Adv. **1**, 042131 (2011).
[19] SWNTs of short lengths were prepared as follows: 0.5 mg of long-SWNT material was suspended in 5 ml of a 3:1 mixture of concentrated 95% sulfuric acid and 59% nitric acid, and then ultrasonicated (44 kHz, ultrasonic intensity about 70 W cm$^{-2}$) for 10, 20, or 30 h at 8 °C.
[20] After ultrasonication, 1 ml of SWNT suspension in acid was diluted with 20 ml distilled water followed by centrifugation at 900g for 2 h. The upper 95% of the supernatant was then carefully decanted and 1 ml of the precipitate containing visible SWNT agglomerates was again diluted with 20 ml of distilled water with subsequent centrifugation for 10 min. This procedure was repeated five times until the pH exceeded 5.0.
[21] J. Liu, A. G. Rinzler, H. Dai, J. H. Hafner, R. K. Bradley, P. J. Boul, A. Lu, T. Iverson, K. Shelimov, C. B. Huffman, F. Rodriguez-Macias, Y.-S. Shon, T. R. Lee, D. T. Colbert, and R. E. Smalley, Science **280**, 1253 (1998).
[22] See Supplemental Material at http://link.aps.org/supplemental/10.1103/PhysRevB.85.165435 for supplementary information.
[23] V. Skakalova, A. B. Kaiser, U. Dettlaff-Weglikowska, K. Hrncarikova, and S. Roth, J. Phys. Chem. B **109**, 7174 (2005).
[24] H. Hu, B. Zhao, M. A. Hamon, K. Kamaras, M. E. Itkis, and R. C. Haddon J. Am. Chem. Soc. **125**, 14893 (2005).
[25] C. Thomsen and S. Reich, Top. Appl. Phys. **108**, 115 (2007).
[26] S. G. Chou, H. Son, J. Kong, A. Jorio, R. Saito, M. Zheng, G. Dresselhaus, and M. S. Dresselhaus, Appl. Phys. Lett. **90**, 131109 (2007).
[27] F. Hennrich, R. Wellmann, S. Malik, S. Lebedkina, and M. M. Kappes, Phys. Chem. Chem. Phys. **5**, 178 (2003).
[28] K. Kamarás, M. E. Itkis, H. Hu, B. Zhao, and R. C. Haddon, Science **301**, 1501 (2003).
[29] S. Tasaki, K. Maekawa, and T. Yamabe, Phys. Rev. B **57**, 9301 (1998).